

A computational study of the coalescence between a drop and an interface in Newtonian and viscoelastic fluids

Pengtao Yue

Department of Chemical and Biological Engineering, University of British Columbia, Vancouver, British Columbia V6T 1Z3, Canada and Department of Mathematics, University of British Columbia, Vancouver, British Columbia V6T 1Z2, Canada

Chunfeng Zhou

Department of Chemical and Biological Engineering, University of British Columbia, Vancouver, British Columbia V6T 1Z3, Canada

James J. Feng^{a)}

Department of Chemical and Biological Engineering, University of British Columbia, Vancouver, British Columbia V6T 1Z3, Canada and Department of Mathematics, University of British Columbia, Vancouver, British Columbia V6T 1Z2, Canada

(Received 1 May 2006; accepted 19 September 2006; published online 25 October 2006)

A drop falling onto a fluid-fluid interface may not merge with it at once but may undergo a so-called partial coalescence cascade. Experimental observations of this phenomenon have revealed fascinating features of the process for Newtonian as well as polymeric fluids. In this paper, we describe numerical simulations of partial coalescence based on a phase-field method. Results show that partial coalescence occurs for an intermediate range of drop sizes, and proceeds in two stages: capillary waves propagating along the drop and transforming it into a fluid column, and neck formation on the column and pinch-off of the secondary drop. In the first stage, interfacial energy turns into kinetic energy following film rupture, while in the second, the kinetic energy overcomes an energy barrier due to the initial increase in interfacial area during neck formation. A parametric study establishes a criterion for partial coalescence in terms of a maximum Ohnesorge number that applies to a wide range of fluid densities and viscosities as long as the Bond number is small. Viscoelasticity in either the drop or the matrix tends to delay the pinch-off of the secondary drop, and may even suppress partial coalescence altogether. The underlying mechanism is large tensile polymer stresses resisting the stretching and thinning of the fluid neck. The numerical results are in qualitative, and in some cases quantitative, agreement with prior experiments. © 2006 American Institute of Physics. [DOI: 10.1063/1.2364144]

I. INTRODUCTION

When a drop settles gently in an immiscible ambient fluid onto a flat interface between these two fluids, it rests on the interface for an extended time and then coalesces with the homophase beneath the interface. The rest time is associated with the drainage of the ambient fluid from the thin film between the drop and the interface, and exhibits a Gaussian-like distribution due to the stochastic nature of film rupture. But the coalescence process is highly repeatable, and occurs on a time scale much shorter than the rest time. Under certain conditions, the merging between the drop and lower bulk is not completed at once but goes through many cycles of *partial coalescence*, each leaving a smaller daughter drop on the interface. This peculiar phenomenon, made widely known by Charles and Mason¹ in 1960, has not been studied nearly as extensively as the film drainage preceding it,^{2,3} and is the focus of this computational study.

To give a brief summary of the experimental findings, it is convenient to define four dimensionless groups that govern the partial coalescence process,

$$\text{Oh} = \frac{\mu_1}{\sqrt{\rho_1 \sigma D}}, \quad (1)$$

$$\text{Bo} = \frac{|\rho_1 - \rho_2| g D^2}{\sigma}, \quad (2)$$

$$\rho^* = \frac{\rho_1}{\rho_2}, \quad (3)$$

$$\mu^* = \frac{\mu_1}{\mu_2}, \quad (4)$$

where D is the diameter of the drop and σ is the interfacial tension. ρ and μ are the density and viscosity of the fluids, with subscripts 1 and 2 denoting the drop and the matrix phase, respectively. The Ohnesorge number Oh and Bond number Bo indicate the relative importance of viscosity and gravity with respect to interfacial tension.

Charles and Mason¹ attributed partial coalescence to capillary pinch-off. Upon film rupture, the primary drop transforms into a liquid column. The column gets thinner in time until Rayleigh instability produces a neck near its base.

^{a)} Author to whom all correspondence should be addressed. Electronic mail: jfeng@CHML.UBC.CA

A secondary drop then pinches off. If one equates the secondary drop size to the wavelength of the fastest-growing capillary wave, this picture implies a constant size ratio between the secondary and primary drops $\zeta=0.42$, somewhat below observed values.^{1,4} Including the viscosity of either component will lead to an even greater underprediction.^{5,6}

Thoroddsen and Takehara⁴ recognized that for low-viscosity fluids such as water and air, there exists an intermediate range of drop size D such that both Oh and Bo are vanishingly small. Then the size ratio ζ can only depend on ρ^* and μ^* , and must remain a constant through successive cycles of partial coalescence. For their fluids, such a self-similar regime was observed for D on the order of hundreds of micrometers, and the constant ζ is around 0.5. More recently, Chen *et al.*² extended this picture by identifying a viscous regime for smaller drops and a gravity regime for larger ones. Scaling relationships have been developed for the size ratio ζ and the coalescence time τ_c in terms of the Bond number Bo and the Ohnesorge number Oh.

A general criterion for the occurrence of partial coalescence has remained elusive. Based on earlier data, Charles and Mason¹ proposed a criterion based on the viscosity ratio: $0.02 < \mu^* < 7-11$. This was later contradicted by Thoroddsen and Takehara,⁴ who observed partial coalescence for water and ethanol drops in air with $\mu^* \sim 100$. Mohamed-Kassim and Longmire⁷ argued that viscosity, gravity, inertia, and capillarity all influence partial coalescence, and suggested a criterion $\text{Bo} \cdot \text{Oh} < 0.02-0.03$, where Oh is an Ohnesorge number defined using the average density and viscosity between the two fluids. This cannot be a universal criterion, however. As $\text{Bo} \cdot \text{Oh} \propto D^{3/2}$, this criterion implies that if partial coalescence occurs for a certain D , it would occur for all subsequent smaller drops. In reality, the partial coalescence cascade terminates for sufficiently small drops when capillary breakup is arrested by viscosity.^{4,8} For low-viscosity liquids, Chen *et al.*² found that partial coalescence occurs for an intermediate range of drop sizes bounded by a critical $\text{Bo}_c \sim 5$ for large drops and by a critical $\text{Oh}_c \sim 0.02$ for small drops.

Finally, the above experiments are all based on Newtonian fluids. Chen *et al.*³ hypothesized that partial coalescence involves strongly extensional deformation of the fluids, and may be sensitive to viscoelasticity. Their experiment has largely confirmed this idea; viscoelasticity in either phase seems to suppress partial coalescence. Without data on the flow and stress fields, however, it is impossible to construct a detailed understanding of the mechanisms at work. A similar statement can be made for the Newtonian experiments as well. Thus, a computational investigation of the partial coalescence process seems highly desirable at present.

Partial coalescence is difficult to simulate because of the morphological changes of the interfaces that occur on exceedingly small time and length scales. In recent years, we have developed a phase-field method for interfacial flows of complex fluids that is capable of handling interfacial rupture and coalescence.⁹ The interface, implicitly represented by a phase-field variable, is modeled as a diffuse layer that stores a mixing energy that gives rise to the interfacial tension. The energy formulation makes it easy to incorporate complex

rheology. Despite successful applications to a variety of problems,¹⁰⁻¹⁹ the phase-field description faces an intrinsic challenge in representing the vastly disparate length scales for the interface and the bulk. Recently, progress has been made by adaptive meshing.^{20,21} Still, it remains to be seen whether the partial coalescence process can be successfully reproduced numerically.

Thus, we have set three objectives for this study: (a) to reproduce quantitatively the partial coalescence process in Newtonian fluids; (b) to establish a more firmly grounded and more general criterion for partial coalescence through a parametric study; and (c) to clarify the effects of viscoelasticity in the process.

The plan for the rest of the paper is as follows. Section II briefly summarizes the mathematical model and numerical methods. Section III presents the main results of the study in three subsections. The first uses *quantitative* comparisons with experiments to demonstrate the capability and limitation of the numerical methods. The second consists of a parametric study that culminates in a criterion for partial coalescence in low-Bond-number situations. The final subsection is devoted to viscoelasticity. Section IV summarizes the main results and points out the limitations of this work.

II. GOVERNING EQUATIONS AND NUMERICAL METHODS

The theoretical model and numerical method used in our computation have been described at length elsewhere,^{9,20,22} and only a brief outline is given here. Consider an immiscible blend of a Newtonian fluid with viscosity μ_n and a viscoelastic Giesekus fluid with solvent viscosity μ_s and polymer viscosity μ_p . We introduce a phase-field variable ϕ to describe the *diffuse interface* between the two components; $\phi=-1$ and 1 in the Newtonian and Giesekus bulk phases, and it changes smoothly across the interfacial layer. The nominal “interface” is at $\phi=0$. The governing equations consist of the Cahn-Hilliard equation describing the convection and diffusion of the interface, the linear momentum equation, the continuity equation, and a constitutive equation for the viscoelastic fluid:

$$\frac{\partial \phi}{\partial t} + \mathbf{v} \cdot \nabla \phi = \gamma \nabla^2 G, \quad (5)$$

$$\rho \left(\frac{\partial \mathbf{v}}{\partial t} + \mathbf{v} \cdot \nabla \mathbf{v} \right) = \nabla \cdot (-p\mathbf{I} + \boldsymbol{\tau}) + G \nabla \phi + \rho \mathbf{g}, \quad (6)$$

$$\nabla \cdot \mathbf{v} = 0, \quad (7)$$

$$\boldsymbol{\tau}_p + \lambda_H \boldsymbol{\tau}_{p(1)} - \alpha \frac{\lambda_H}{\mu_p} (\boldsymbol{\tau}_p \cdot \boldsymbol{\tau}_p) = \mu_p [\nabla \mathbf{v} + (\nabla \mathbf{v})^T], \quad (8)$$

where

$$G = \lambda \left[-\nabla^2 \phi + \frac{\phi(\phi^2 - 1)}{\epsilon^2} \right] \quad (9)$$

is the chemical potential, γ is the Cahn-Hilliard mobility parameter, ϵ is the capillary width, λ is the mixing energy

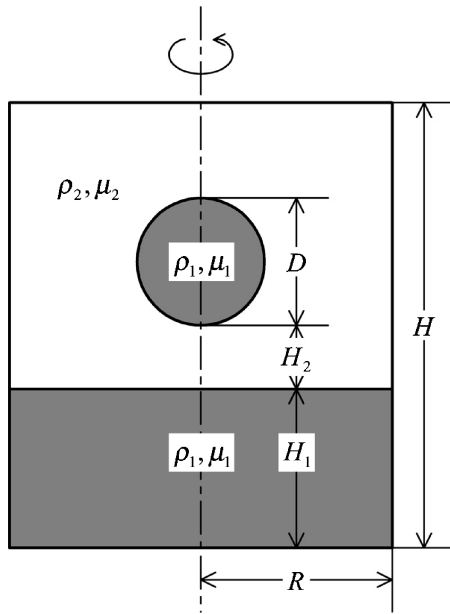


FIG. 1. A schematic of the geometry of the numerical simulation. Because of axisymmetry, the computational domain is the right half of the meridian plane.

that determines the interfacial tension:⁹ $\sigma = \frac{2\sqrt{2}\lambda}{3\epsilon}$. The total stress tensor is

$$\tau = \left(\frac{1+\phi}{2}\mu_s + \frac{1-\phi}{2}\mu_n \right) [\nabla\mathbf{v} + (\nabla\mathbf{v})^T] + \frac{1+\phi}{2}\tau_p, \quad (10)$$

where τ_p is the polymer stress. λ_H is the polymer relaxation time, α is the mobility parameter in the Giesekus model,²³ and the subscript ₍₁₎ denotes the upper convected derivative. The Oldroyd-B model is recovered when $\alpha=0$. The density ρ is the average between the two components using their “concentrations” $\frac{1\pm\phi}{2}$, and \mathbf{g} is the gravitational acceleration.

Equations (5)–(8) are solved by a finite-element code AMPHI that uses adaptive meshing to resolve the narrow interface.²⁰ P2 elements are used for \mathbf{v} and ϕ , and P1 elements for p and τ_p . Second-order implicit schemes are used for temporal discretization. A general-purpose mesh generator GRUMMP²⁴ is adopted for the adaptive meshing, and ϕ is used as the criterion of mesh refinement. The most challenging aspect of the computation is in resolving the interfacial region, which has a thickness $\sim 5\epsilon$, and the attendant numerical issues have been discussed in previous publications.^{20,22} Extensive numerical experiments have determined the ranges of the time step and grid size required for adequate resolution. All the results presented here satisfy these guidelines.

III. RESULTS AND DISCUSSIONS

We assume an axisymmetric geometry for the partial coalescence process as illustrated in Fig. 1. The rectangular computational domain has $H=7D$ and $R=3D$. The depth of the lower bulk $H_1=3D$, and we initially place the drop very close to the flat interface, $H_2=0.02D$. The capillary width $\epsilon=0.005D$, and the mesh size is 0.8ϵ at the interface and $0.2D$ in the bulk phases. All quantities are made dimensionless by

D , ρ_1 , and σ . In particular, the characteristic time is the inertio-capillary time $t_{ic}=(\rho_1 D^3/\sigma)^{1/2}$, and stresses are scaled by σ/D . The four dimensionless groups have been given in the Introduction. For boundary conditions, we set the velocity $\mathbf{v}=0$ at the lower and right boundaries, and impose symmetry conditions along the axis. On the upper boundary, we impose the natural boundary condition of vanishing stresses. The initial condition is $\mathbf{v}=0$ everywhere.

The mobility parameter γ needs to be chosen carefully such that the Cahn-Hilliard diffusion maintains the interfacial profile without overly damping the flow field.¹³ With $\epsilon=0.005D$ fixed, varying γ [scaled by $D^3/(t_{ic}\sigma)$] from 2.5×10^{-5} to 4.0×10^{-4} results in less than 1% variation in the drop size ratio. In most simulations, therefore, we have used $\gamma=1.0 \times 10^{-4}$. Furthermore, we have tested other values of the capillary width: $\epsilon=0.004D$, $0.01D$, and $0.02D$. γ is changed accordingly in proportion to ϵ^2 as suggested by Jacqmin,¹³ from 6.4×10^{-5} to 1.6×10^{-3} . For $\epsilon=0.004D$ and $0.01D$, the results differ from that for $\epsilon=0.005D$ by less than 0.2%, while for $\epsilon=0.02D$, the difference is roughly 3%. Thus, $\epsilon=0.005D$ gives an interface thin enough to guarantee converged results.

For a typical run, the adaptive mesh has $2 \times 10^4 \sim 3 \times 10^4$ cells, with about $1.7 \times 10^5 \sim 2.6 \times 10^5$ unknowns. The time step is chosen such that the interface will not move over one mesh cell at one step,²⁰ and ranges from 10^{-4} to 10^{-2} in dimensionless terms. Typically, one cycle of partial coalescence takes less than 2000 time steps, and requires less than 12 h of computation on a 3.0G Xeon processor.

A. Newtonian fluids: Comparison with experiments

Prior experiments^{1,2,4,7} made two important observations on partial coalescence: (a) The process consists of two stages, namely the propagation of capillary waves up the surface of the drop and capillary breakup of the filament that produces the daughter drop; (b) partial coalescence occurs for an intermediate range of drop sizes, and is arrested by gravity for larger drops and by viscosity for smaller ones. Those have been reproduced, quantitatively for the most part, by our simulations.

As an experimental benchmark, we have chosen the sequence in Fig. 4 of Chen *et al.*² showing a water drop coalescing with an oil-water interface. The oil-based matrix fluid is 20% polybutene in decane. The dimensional parameters are $D=1.1$ mm, $\sigma=29.7$ dyn/cm, $\rho_1=1.0$ g/cm³, $\mu_1=0.01$ poise, $\rho_2=0.76$ g/cm³, and $\mu_2=0.02$ poise. The dimensionless parameters are $Oh=5.53 \times 10^{-3}$, $Bo=9.58 \times 10^{-2}$, $\rho^*=1.32$, and $\mu^*=0.5$. We have also simulated an experiment by Charles and Mason¹ on partial coalescence of a water drop with an interface with aniline. The outcome of the comparison is almost identical to the one described here.

Figure 2 shows a frame-by-frame comparison of the interfacial evolution during partial coalescence. First, the oil film between the drop and the interface ruptures at $t=0$, and this sets off surface waves that propagate up the drop surface and outward on the interface [(a)–(d)]. In time the drop is transformed into a fluid column that shrinks in diameter continuously [(e)–(h)]. The height of the column does not dimin-

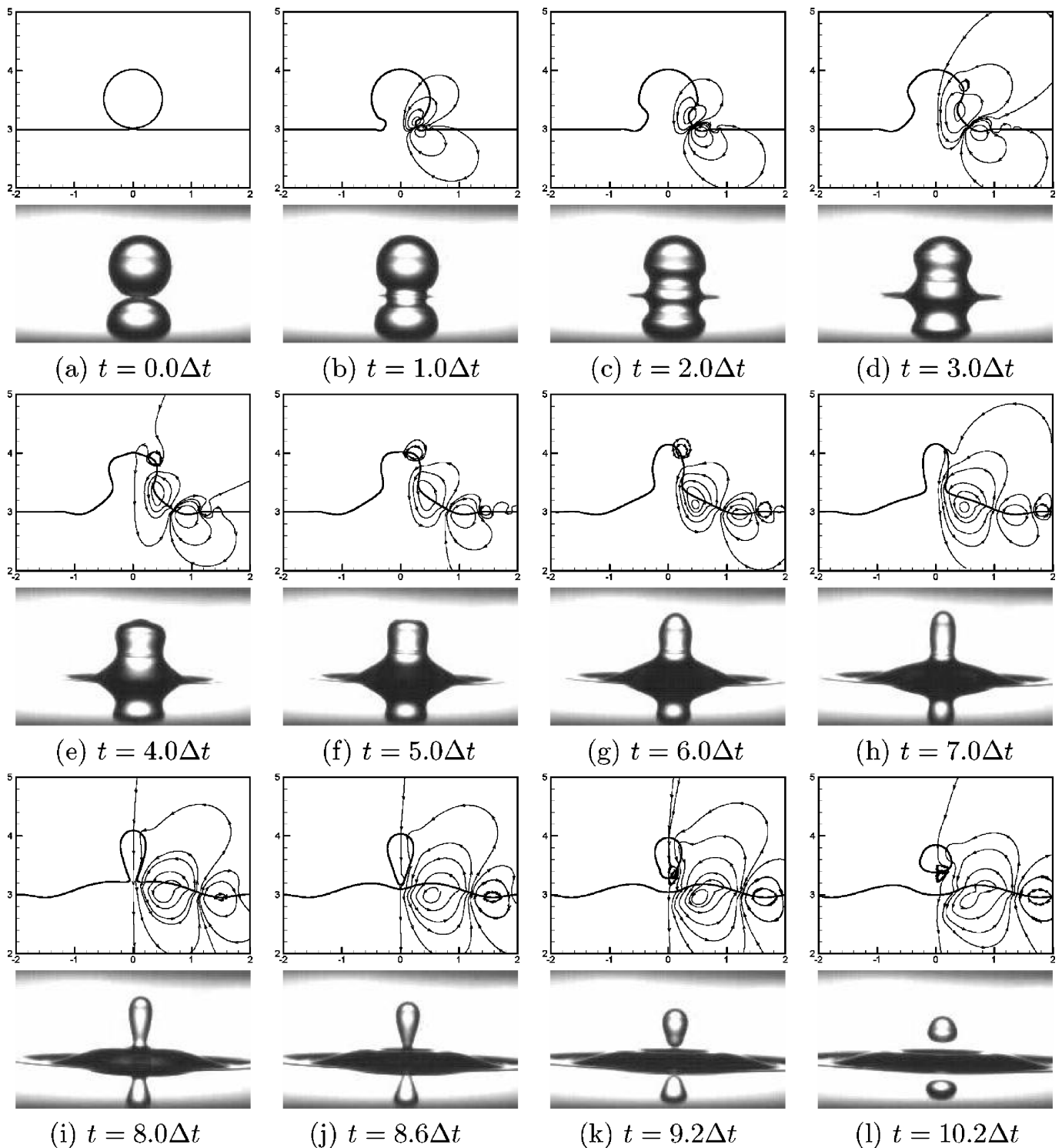


FIG. 2. Comparison between numerical and experimental results for a partial coalescence cycle. The time interval between experimental snapshots (lower rows) is fixed: $\Delta t = 542 \mu\text{s}$, and the times indicated are those at which the numerical picture resembles the experimental one most closely. Instantaneous streamlines are plotted on the right half of the numerical pictures (enhanced online).

ish at this stage, however. In fact, the column lengthens somewhat. Now a neck forms at the bottom of the column and continues to pinch in (i). Finally, pinch-off occurs (j) and a secondary drop is left above the interface [(k),(l)].

The simulation not only captures the qualitative features of partial coalescence, but also predicts the interfacial shape and drop size with *quantitative* precision. The only discrep-

ancy is with the time intervals between (i), (j), and (k): the pinch-off of the filament at the neck and the formation of the secondary drop occur faster in the simulation than in the experiment. In a microscopic view, pinch-off happens when the distance between interfaces becomes comparable to the interfacial thickness and the van der Waals force begins to dominate. In reality, the oil-water interface spans tens of na-

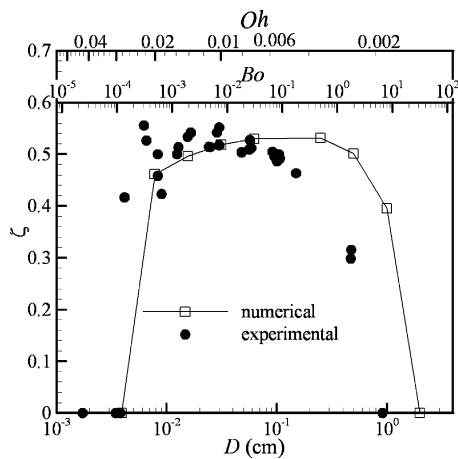


FIG. 3. Drop size ratio ζ vs initial drop size D in a water/decane system. For the decane matrix $\rho_2=0.74$ g/cm³, $\mu_2=0.01$ poise, and $\sigma=32$ dyn/cm. The filled circles are from experiments of Chen *et al.* (Ref. 2).

nometers. In our phase-field model, however, ϵ is much larger. This is a numerical necessity as it is computationally prohibitive to resolve the range of length scales from $D \sim 1$ mm down to nanometers. The thicker interface then leads to earlier interfacial rupture and coalescence. Note that this issue only affects portions of the simulation that involve short length scales. Adaptive meshing has allowed resolution of thinner interfaces,²⁰ and numerical effects due to Cahn-Hilliard diffusion can be minimized by a judicious choice of phase-field parameters.^{9,25}

It is instructive to examine the interchange among interfacial, kinetic, and potential energies during the partial coalescence. The onset and propagation of surface waves in Figs. 2(b)–2(d) involves mostly interfacial energy being transformed into kinetic energy of the two fluids. Some of this kinetic energy turns into potential energy when the upward momentum lifts the top of the liquid column in (h). In Fig. 2(h), the height-to-diameter ratio of the fluid column is approximately 2, smaller than π that is required for surface perturbations to grow according to Plateau's capillary instability.²⁶ This means that the interfacial area (and energy) will increase if a neck is formed. Thus the necking, at least initially, is driven by inertia as the kinetic energy is trans-

formed back into interfacial energy. If the velocity is suddenly set to zero at the beginning of necking, no pinch-off would occur.²⁷ The increase of interfacial area presents an *energy barrier* that has to be overcome for partial coalescence to occur. This point will be revisited when we investigate the critical conditions for partial coalescence.

Partial coalescence occurs for an intermediate range of drop diameters, and this is depicted in Fig. 3 in terms of the drop size ratio ζ . Note that $\zeta=0$ implies complete coalescence. The computational parameters correspond to experiments on water drops in a decane matrix,² and the experimental data are also shown for comparison. Numerical results show a range of the drop diameter D within which $\zeta > 0$. The upper bound D_u lies between 1 and 2 cm (these are the two runs that straddle the boundary), and the lower bound D_l is between 39 and 78 μm . The range $D_l < D < D_u$ can be recast in terms of Oh and Bo , and these two parameters are also shown in the figure.

When D decreases, Oh increases and so does the significance of viscosity. As $D \rightarrow D_l$, the surface waves will be dampened by viscosity to such an extent that no pinch-off occurs. Such a scenario is depicted in Fig. 4. In a separate simulation for a larger drop ($D=312.5$ μm , $Oh=9.96 \times 10^{-3}$), partial coalescence does occur; the neck forms on the liquid column at dimensionless time $t=0.56$ and the secondary drop pinches off at $t=0.70$. In comparison, the neck formation in Fig. 4(b) is delayed by the viscous effect at the greater Oh . Consequently, more kinetic energy is dissipated prior to neck formation, and what remains is not enough to overcome the energy barrier due to the increase in interfacial area that a pinch-off would entail. The result is complete coalescence. Thus, viscous dissipation determines whether the energy barrier can be surmounted. If it is, however, viscosity exerts only a weak influence in the ensuing partial coalescence process since $Oh \sim 10^{-2}$ is much below unity. Therefore, the drop size ratio remains roughly a constant ($\zeta \sim 0.5$) with increasing Oh until the kinetic energy fails to negotiate the barrier. At that point ζ plummets to zero and partial coalescence is arrested. The precipitous transition at D_l , as opposed to the gradual one at D_u , is a signature of the energy barrier.

On the opposite end of the D range, gravity begins to

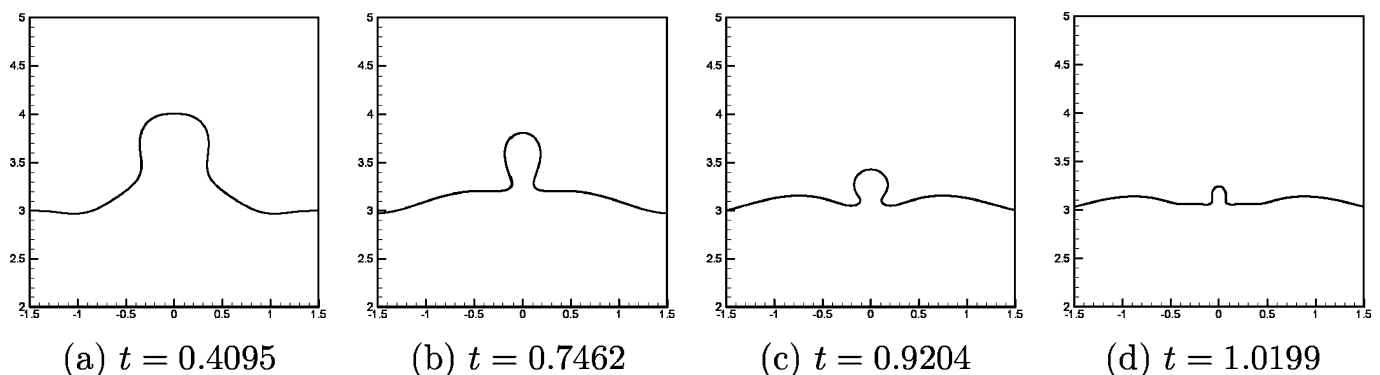


FIG. 4. Partial coalescence is arrested by viscosity for a drop of diameter $D=39$ $\mu\text{m} < D_l$. The material properties are for a water-in-decane system, $Oh=2.82 \times 10^{-2}$, and t is made dimensionless by the inertia-capillary time t_{ic} (enhanced online).

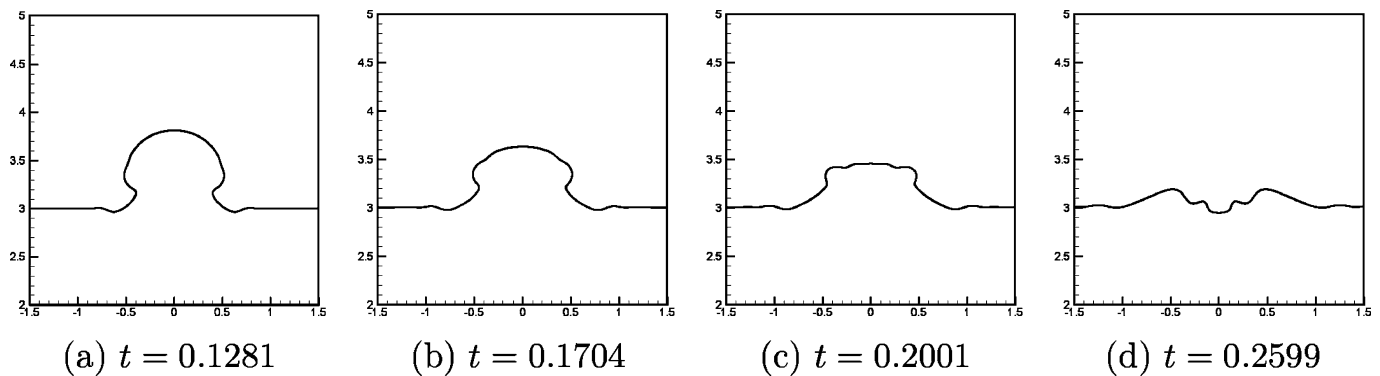


FIG. 5. Partial coalescence is arrested by gravity for a drop of diameter $D=2\text{ cm}>D_u$. The material properties are for a water-in-decane system, $Bo=31.9$, and t is made dimensionless by the inertio-capillary time t_{ic} (enhanced online).

dominate as D (or Bo) increases, and this produces a faster depletion of the drop. Figure 5 shows a simulation for a water drop in decane whose diameter is just above D_u . Under gravity, the drop fluid drains so fast into the lower bulk phase that the whole drop practically collapses before the neck has time to form. Thus, partial coalescence is arrested by gravity for large drops.

Furthermore, the numerical results in Fig. 3 show the three regimes of partial coalescence previously identified in experiments: an inertio-capillary regime with a constant ζ sandwiched by a viscous regime (for smaller drops) and a gravity regime (for larger drops) where ζ is reduced, respectively, by viscous dissipation and gravity-driven drainage, eventually to zero. More quantitatively, the simulation reproduces D_l almost exactly. The predicted ζ agrees with experimental data fairly well for $Bo<0.1$. For larger drops, however, the simulation overpredicts ζ and D_u . The reason is that the initial condition used in the simulations—a spherical drop a small distance above a flat interface—does not reflect the real geometry of the interfaces just prior to film rupture, especially at high Bo . In reality, coalescence is preceded by a relatively slow film-drainage process. During this time, the drop and the interface deform under gravity when Bo is large. The drop sags into an ellipsoidal shape that minimizes the sum of interfacial and potential energies.⁷ Meanwhile, the interface beneath the drop becomes highly curved for the interfacial tension to provide an upward net force that bears the weight of the drop. Thus, the drop “makes contact” with the interface over a much larger area than the wedge between a sphere and a flat interface [cf. Fig. 2(a)]. Once the film ruptures, a wider conduit opens and the drop fluid drains out more readily than in our numerical simulations. This explains the high- Bo discrepancy in Fig. 3.

To capture the film drainage process and the curved interfaces at large Bo is difficult because of the inherent limitation of our phase-field method. The relatively thick diffuse interface tends to cause coalescence to occur prematurely as compared to reality. It is a challenge for any numerical model to accommodate the three disparate length scales: $D\gg$ film thickness \gg interface thickness, and especially so for interface-capturing methods. To our knowledge, the only attempt to simulate the film drainage between a drop and an interface using interface capturing is by Zheng *et al.*,²⁸ with

the level-set method. It is fortunate that this issue does not affect partial coalescence for smaller Bo , where a spherical drop above a flat interface is a good enough geometric approximation.

To sum up, we have used well-characterized experiments to benchmark our numerical scheme AMPHI. It gives accurate predictions except for two processes—initial film rupture and pinch-off of the daughter drop—where the small separation between interfaces taxes the diffuse-interface method. The first precludes us from studying the film drainage process and limits us to small Bo values for the rest of the paper, and the second must be kept in mind as a caveat in interpreting numerical results.

B. Newtonian fluids: Parametric study

1. Effect of the Bond number Bo

To assess the uncertainties related to the initial interfacial shape at large Bo , we first quantify the effect of Bo . Figure 6 shows the variation of ζ with Bo at fixed Oh , ρ^* , and μ^* . Note that this plot differs from Fig. 3 where all material constants are fixed and the drop diameter D changes. Here, one may think of D as being fixed as well, and Bo being varied by changing g . For $Bo<0.1$, ζ is essentially independent of Bo as the gravity effect becomes insignificant. For decreasing Oh , ζ is seen to converge to the

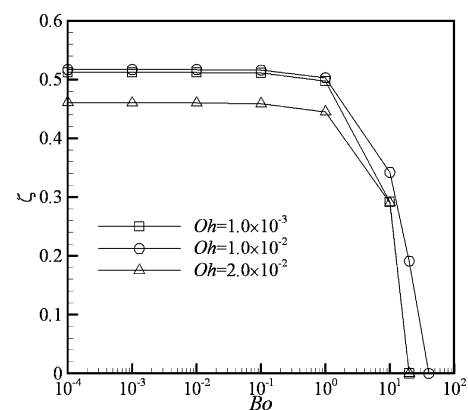


FIG. 6. Drop size ratio ζ as a function of Bo for several Oh values. Density ratio $\rho^*=1.33$, viscosity ratio $\mu^*=1$.

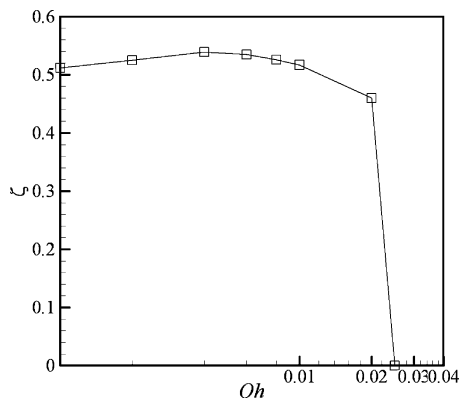


FIG. 7. Drop size ratio ζ as a function of Oh with the other parameters fixed: $Bo=10^{-3}$, $\mu^*=1$, $\rho^*=1.33$. The same trend is observed for other μ^* values tested, both below and above unity.

plateau value in Fig. 3 that characterizes the inertio-capillary regime.^{2,4} On the other hand, if Oh increases to a critical value near 2.5×10^{-2} , ζ abruptly drops to zero for all Bo because of the energy barrier explained before. With increasing Bo , ζ decreases to zero gradually in the gravity regime, in which our numerical results are subject to increasing errors. Therefore, all simulations presented hereafter have used $Bo=10^{-3}$ with negligible gravity effect. In reality, this small Bo corresponds to a small drop (roughly $D \leq 100 \mu\text{m}$ in Fig. 3) or a small density difference between the two fluids or even microgravity.

2. Effect of the Ohnesorge number Oh

With the three other dimensionless parameters fixed, the effect of varying Oh may be thought of as due to changing the viscosities μ_1 and μ_2 in proportion. Figure 7 depicts the variation of the drop size ratio ζ in such a scenario.

The drop size ratio ζ is not a monotonic function of Oh but achieves a maximum at an intermediate Oh . This non-monotonicity can be attributed to the competition between drop depletion and pinch-off at the neck. Note first that the curve approaches the inertio-capillary regime on the left as $Oh \rightarrow 0$. With increasing Oh , viscous dissipation hampers the downward flow of the drop fluid that depletes the drop. As a result, less fluid drains out of the drop and ζ tends to increase with Oh .

In the meanwhile, viscosity also dampens the development of surface disturbances that will eventually lead to the pinch-off of the liquid column, as in Figs. 2(g)–2(j). This can be more precisely shown by measuring the coalescence time τ_c , defined as the interval between the initial film rupture and the pinch-off of the secondary drop. Figure 8(a) plots the dependence of τ_c , scaled by the inertio-capillary time t_{ic} , on viscosity of the two components represented by an average Ohnesorge number, $\overline{Oh} = \bar{\mu} / \sqrt{\bar{\rho}\sigma D}$, where $\bar{\mu} = (\mu_1 + \mu_2)/2$ and $\bar{\rho} = (\rho_1 + \rho_2)/2$. The increase of τ_c with \overline{Oh} (or the viscosity of either component) confirms the viscous damping of the growth of surface disturbances. Thus, more fluid tends to drain out of the drop before the pinch-off. This effect apparently dominates the reduction in draining speed at higher Oh , and causes ζ to decrease with Oh . Thus the viscous regime is obtained,² and eventually ζ drops to zero as Oh approaches a critical value.

Incidentally, the τ_c results in Fig. 8(a) seem to contradict Kinoshita *et al.*'s theory on viscous damping of capillary instability on a fluid filament.²⁹ When a small amount of viscosity is added to either the filament or the matrix, it serves as a perturbation to Rayleigh's inviscid theory, and a linear increase of the pinch-off time with Oh is expected. However, Kinoshita *et al.* showed that the viscosity of the filament μ_1 has more impact than the matrix viscosity μ_2 , and the two should be combined as $\mu' = (3\mu_1 + \mu_2)/4$ in constructing the Ohnesorge number. It is surprising that our data for a wide range of μ^* are successfully represented by the average viscosity $\bar{\mu}$, but not by μ' [Fig. 8(b)]. This may be rationalized by the fact that our liquid column is not an infinite filament in a quiescent matrix; instead, there are complex flow fields in and surrounding the column, and the kinetic energy of the drop fluid has to overcome the aforementioned energy barrier in effecting a pinch-off.

The linear fitting yields $\tau_c = 0.634$ at the limit of $\overline{Oh} = 0$ where the process is totally determined by capillarity and inertia. This compares with the experimental value $\tau_c \approx 0.70$ in the inertio-capillary regime.² Again, the under-prediction is due to premature pinch-off in our diffuse-interface model.

3. Effect of the viscosity ratio μ^*

With all other parameters fixed, varying μ^* amounts to varying the matrix viscosity μ_2 while keeping the drop vis-

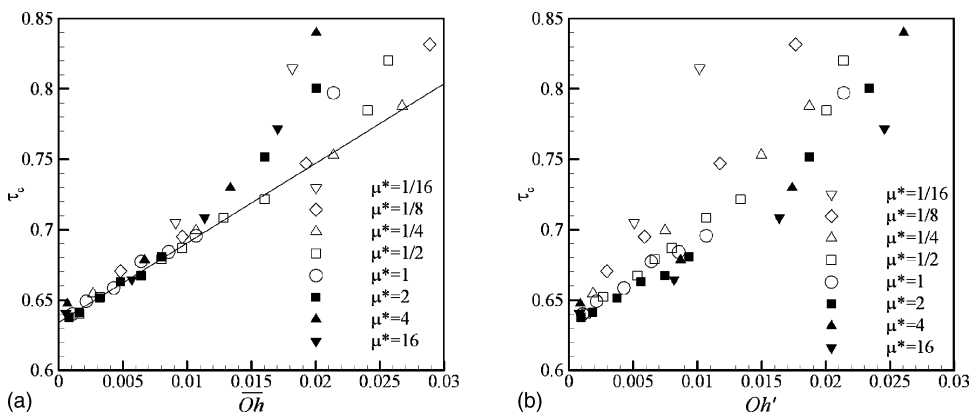


FIG. 8. Coalescence time τ_c increases with the viscosity of either fluid component. (a) Plotted against \overline{Oh} , data at various viscosity ratios tend to collapse onto a single line for small \overline{Oh} . The solid line, $\tau_c = 0.634(1 + 8.920\overline{Oh})$, is the linear fitting of three sets of data at $\mu^* = 1/2, 1, 2$, and $\overline{Oh} \leq 0.01$. (b) No such collapse occurs if data are plotted against Oh' defined using $\mu' = (3\mu_1 + \mu_2)/4$ as suggested by Kinoshita *et al.* (Ref. 29).

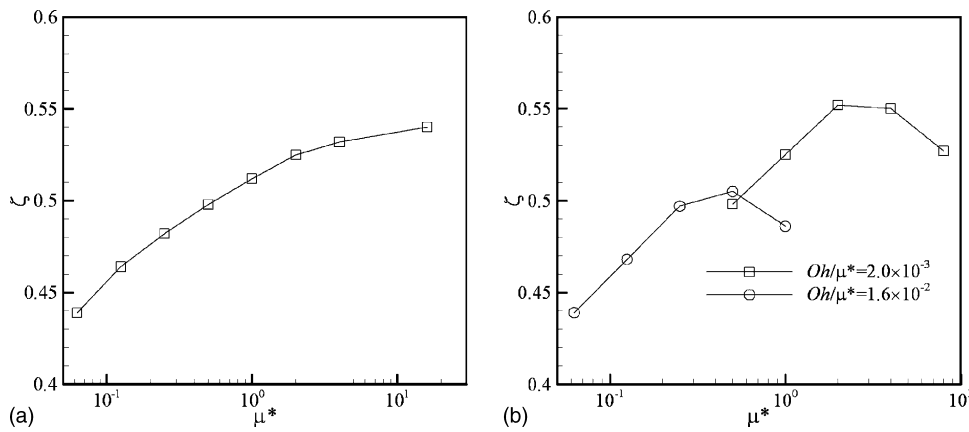


FIG. 9. The drop size ratio ζ as a function of the viscosity ratio μ^* (a) at fixed $Oh=10^{-3}$; (b) at fixed Oh/μ^* . The other parameters are $Bo=10^{-3}$ and $\rho^*=1.33$.

cosity μ_1 constant. Thus, the draining speed of the drop fluid should not change greatly. With an increasing μ^* , the viscosity of the surrounding fluid is reduced, resulting in a smaller average Ohnesorge number \overline{Oh} . From Fig. 8, we expect a shorter τ_c as the capillary disturbance grows more rapidly. Therefore, the drop size ratio ζ is greater at higher μ^* , as shown by Fig. 9(a). Moreover, since the matrix viscosity scales with $1/\mu^*$, its influence should diminish for large μ^* . This explains the fact that $\zeta(\mu^*)$ levels off with increasing μ^* . One expects ζ to approach an upper limit when $\mu^* \rightarrow \infty$.

To isolate the effect of the drop viscosity μ_1 , we can vary μ^* for a fixed value of Oh/μ^* . Figure 9(b) shows a nonmonotonic variation of ζ , which confirms the argument put forth to explain Fig. 7. In other words, increasing drop viscosity damps the velocity of drainage flow on the one hand, and prolongs the coalescence time on the other. Depending on the competition of these two effects, ζ increases with μ_1 (or μ^* in this case) at smaller μ_1 , peaks, and then declines at higher drop viscosity. The fact that ζ decreases with increasing Oh/μ^* is due to the same effect of the matrix viscosity μ_2 as shown in Fig. 9(a).

4. Effect of the density ratio ρ^*

With all other parameters fixed, ρ^* is varied through the density of the matrix phase ρ_2 . We should mention that when ρ^* crosses unity, the direction of gravity is reversed in the simulations. Results show that ζ increases with ρ^* monotonically [Fig. 10(a)]. As the density and viscosity of the drop fluid are fixed, we can assume that the drainage speed at which the drop is depleted is approximately constant. Then the increase in ζ with ρ^* must be due to a decrease in the coalescence time τ_c , which is indeed the case [Fig. 10(b)]. Owing to the weak viscous effect ($Oh \ll 1$), τ_c scales with an inertia-capillary time $(\rho D^3/\sigma)^{1/2}$, where ρ is a certain combination of ρ_1 and ρ_2 . When ρ^* increases, ρ_2 decreases, and so do ρ and τ_c . The last two data points for $Oh=2 \times 10^{-2}$ are anomalous because this Oh is very close to the maximum Oh for partial coalescence (cf. Fig. 3). Thus, the trends in Fig. 10 are clearly explained.

With $\rho^* \rightarrow \infty$ and the matrix fluid becoming inertialess, ζ tends to an upper limit. When ρ^* decreases, on the other hand, ζ appears to approach zero at a finite critical value ρ_c^* where partial coalescence is arrested by the inertia of the

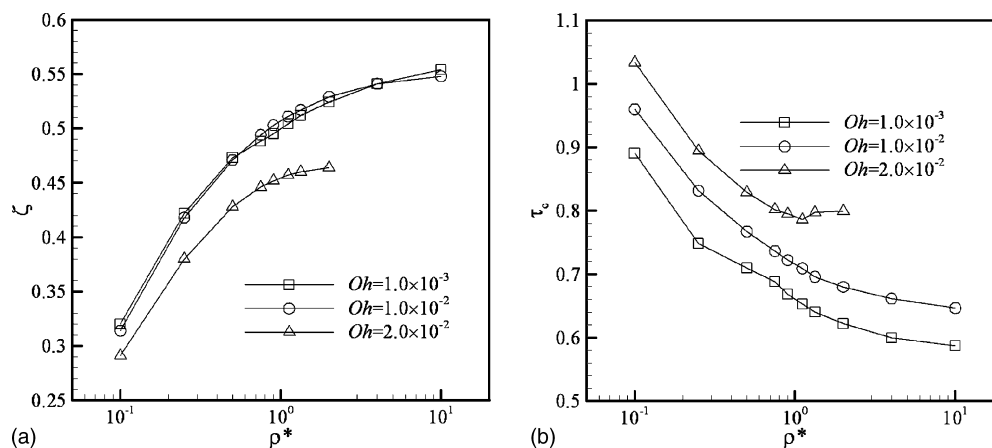


FIG. 10. (a) The drop size ratio ζ increases with the density ratio ρ^* for three fixed values of Oh . (b) The coalescence time τ_c decreases with ρ^* . The other parameters are $\mu^*=1$ and $Bo=10^{-3}$.

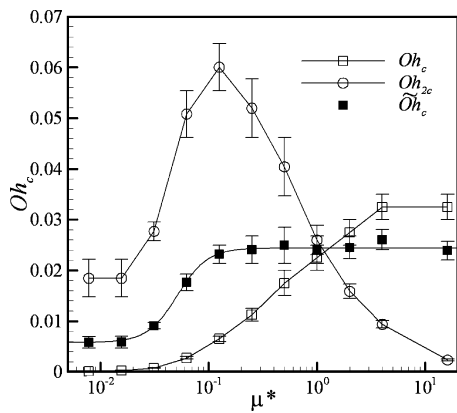


FIG. 11. Dependence of the critical Ohnesorge number on viscosity ratio μ^* at $\rho^* = 1.33$ and $Bo = 10^{-3}$. $Oh_2 = \mu_2 / \sqrt{\rho_2 \sigma D}$ is an Ohnesorge number based on the matrix fluid properties and $\tilde{Oh} = \tilde{\mu} / \sqrt{\bar{\rho} \sigma D}$ is based on a “composite viscosity” $\tilde{\mu} = (2\mu_1 + \mu_2) / 3$.

surrounding fluid. Extrapolation of the curves in Fig. 10(a) indicates a common $\rho_c^* \approx 0.006$ for all Oh values. This ρ_c^* , along with a critical Oh , forms part of a criterion for partial coalescence.

5. Criteria for partial coalescence

Of the four dimensionless groups of the problem, we cannot explore large Bond numbers owing to numerical limitations discussed before. Thus, it seems reasonable to seek a criterion for partial coalescence embodied by a critical Ohnesorge number Oh_c that depends on ρ^* and μ^* . Figure 3 indicates a maximum Oh for partial coalescence, determined in part by the energy barrier. A similar critical Oh_c has been identified for other values of μ^* and ρ^* .

Figure 11 shows the critical Ohnesorge number as a function of μ^* . As Oh is defined using the drop viscosity, we have also plotted the critical condition in terms of a “matrix Ohnesorge number” $Oh_2 = \mu_2 / \sqrt{\rho_2 \sigma D}$. Note first that Oh_c approaches a constant around 3.25×10^{-2} as μ^* increases beyond 4. This is when the matrix viscosity becomes negligible. Conversely, Oh_{2c} approaches a constant near 1.85×10^{-2} when μ^* falls below $1/64$, when the drop viscosity

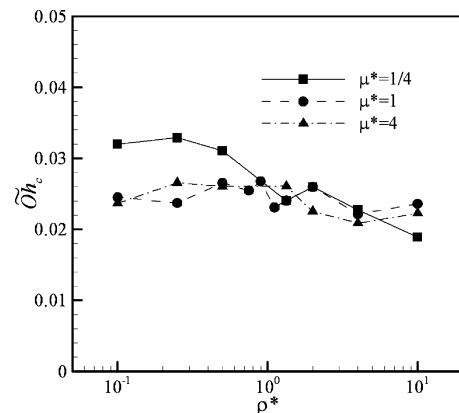


FIG. 12. The critical Ohnesorge number \tilde{Oh}_c depends weakly on ρ^* for an intermediate range of μ^* .

becomes too small to affect the coalescence process. In the intermediate range $1/64 < \mu^* < 4$, both drop and matrix viscosities are important, and the partial coalescence criterion is perhaps best expressed by some combination of μ_1 and μ_2 . After some trial and error, we have found $\tilde{\mu} = (2\mu_1 + \mu_2) / 3$ to be a particularly suitable “composite viscosity”: the critical values of the corresponding Ohnesorge number $\tilde{Oh} = \tilde{\mu} / \sqrt{\bar{\rho} \sigma D}$ exhibit a simple sigmoidal shape on the semilog scale of Fig. 11, and can be fitted to

$$\tilde{Oh}_c(\mu^*) = 2.45 \times 10^{-2} - \frac{1.74 \times 10^{-6}}{\mu^{*3.125} + 9.35 \times 10^{-5}}. \quad (11)$$

The dependence of the critical Ohnesorge number \tilde{Oh}_c on ρ^* is depicted in Fig. 12 for several values of μ^* . For $\mu^* = 1$, \tilde{Oh}_c is nearly a constant over the range of ρ^* tested. This implies that in this case the inertia of both phases exerts equal influence on the criterion for partial coalescence, such that as long as $\bar{\rho}$ is used to calculate the Ohnesorge number, its critical value is insensitive to ρ^* . For the other μ^* values, the variation with ρ^* is very mild as well.

Over wider ranges of ρ^* and μ^* , it is not easy to express the function $\tilde{Oh}_c(\mu^*, \rho^*)$ in an analytical form as Eq. (11). Instead, Fig. 13 depicts this function graphically. Note first

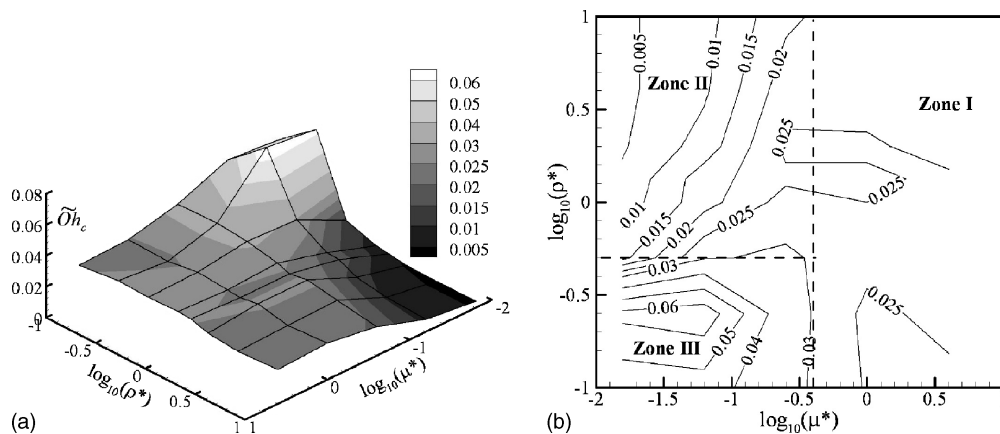


FIG. 13. Critical Ohnesorge number \tilde{Oh}_c as a function of μ^* and ρ^* in a surface plot (a) and a contour plot (b). The former gives a better global view while the latter is more convenient for quantitative evaluation.

that \tilde{Oh}_c is nearly a constant (close to 2.45×10^{-2}) for $\mu^* > 0.4$ (zone I), consistent with prior observations in Fig. 12. In zone II ($\rho^* > 0.5$ and $\mu^* < 0.4$), \tilde{Oh}_c depends on ρ^* weakly and the contours are mostly vertical. Therefore, in zone I and zone II, Eq. (11) is a rather accurate criterion for partial coalescence. These two regions cover most experiments in the literature, especially those on liquid-liquid systems whose ρ^* and μ^* do not deviate greatly from unity.

In zone III ($\rho^* < 0.5$ and $\mu^* < 0.4$), \tilde{Oh}_c depends on both μ^* and ρ^* in a complex way and we did not attempt to fit the data to an empirical equation. The most notable feature is a ridge-like structure roughly parallel to the μ^* axis. This illustrates the fact that for small enough drop viscosity, \tilde{Oh}_c no longer depends on μ^* . The same limiting behavior has been noted in Fig. 11. We should point out that the \tilde{Oh}_c values for small ρ^* and μ^* are subject to greater numerical uncertainty. The reason is that ζ becomes very small in this limit, and numerical resolution of the small secondary drop becomes difficult in our diffuse-interface framework.

Toward the bottom of zone III, there is an additional constraint on partial coalescence: $\rho^* > \rho_c^*$, where $\rho_c^* \approx 0.006$ from extrapolating Fig. 10(a). The physical mechanism underlying ρ_c^* differs from that for the critical Ohnesorge number. \tilde{Oh}_c marks the sudden drop of ζ from a relatively large value to zero, and is determined by the energy barrier. On the other hand, ρ_c^* represents the competition between the coalescence time τ_c , which is roughly the time needed for pinching off the secondary drop, and the time needed for depleting the primary drop. Figure 13(b) shows that for a small ρ^* above ρ_c^* , say $\rho^* = 0.1$, the critical \tilde{Oh}_c for partial coalescence is actually higher than that at a large ρ^* , say $\rho^* = 0.5$. Thus, \tilde{Oh}_c and ρ_c^* are independent constraints.

In summary, we propose $\tilde{Oh}_c(\mu^*, \rho^*)$ in Fig. 13 and $\rho^* > \rho_c^*$ as a “universal” criterion for partial coalescence in Newtonian systems for all density and viscosity ratios. For moderate parameter values in zone I and zone II, the simpler criterion of Eq. (11) may be used. Of course, this criterion is not truly universal because of the small-Bo limitation. Experimentally, Chen *et al.*^{2,3} identified a critical condition $Bo \lesssim 5$ for partial coalescence in the gravity regime. Our simulation seems to suggest the same phenomenon (cf. Fig. 3) but cannot compute the critical Bo with confidence. Furthermore, Mohamed-Kassim and Longmire⁷ noted intermediate regimes where the critical condition for partial coalescence depends on both viscosity and gravity, and suggested the criterion $Bo\tilde{Oh} < 0.02-0.03$. In a way, our criterion complements these large-Bo criteria. It represents a step toward a complete understanding of partial coalescence, but is certainly not the final word on it.

6. Comparison with experiments

When discussing Fig. 3, we have already noted the good agreement of ζ and Oh_c with experimental data for a water/decane system² with ρ^* and μ^* both close to unity. The more general predictions in the parametric study can be compared with other experiments.

For water drops coalescing with an air/water interface, we have $\rho^* \sim 10^3$ and $\mu^* \sim 10^2$. Extrapolating the curves in Figs. 9(a) and 10(a), we may estimate a limiting value $\zeta \approx 0.55$ for large ρ^* and μ^* when Oh is well below the critical value. Thoroddsen and Takehara⁴ observed $\zeta \approx 0.5$ for an air/water system. Honey and Kavehpour⁸ further reported $\zeta = 0.65 \pm 0.08$, 0.58 ± 0.06 , and 0.52 ± 0.05 for methanol, water, and silicone oil drops coalescing with the air/liquid interface. Most recently, Blanchette and Bigioni²⁷ suggested $\zeta \sim 0.55$ at vanishing Bo based on experiments and simulations on an air/ethanol system. For liquid-liquid systems, Charles and Mason¹ experimented with a large variety of immiscible fluid pairs, with $\rho^* \sim 1-11$ and $\mu^* \sim 0.004-70$. Because of the large initial drop size ($D \sim 0.4-0.7$ cm), the Bond number is large ($Bo \geq 1$) and the first cycle of partial coalescence exhibits a small size ratio in the range of 0.13–0.41. In subsequent cycles with smaller D and Bo, they reported $\zeta \approx 0.5 \pm 0.05$. All these data agree well with our predictions.

For liquid drops coalescing with an air/liquid interface, extrapolating Fig. 13 gives a critical $\tilde{Oh}_c \approx 0.025$. The numerical and experimental results of Blanchette and Bigioni²⁷ give $\tilde{Oh}_c = 0.017$ for both water and ethanol, reasonably close to our prediction. If we consider the inverse scenario of an air bubble coalescing with a water/air interface, $\rho^* \approx 1.29 \times 10^{-3}$ and $\mu^* \approx 1.82 \times 10^{-2}$. Since ρ^* is below $\rho_c^* = 0.006$, we expect no partial coalescence. This seems empirically true, and there are no experimental reports to the contrary. Finally, we may rationalize the partial coalescence criterion of Charles and Mason¹ based on the viscosity ratio, $0.02 < \mu^* < 7 \sim 11$. We know that when μ^* is too low or too high, the composite viscosity $\tilde{\mu}$ is dominated by the larger of the two viscosities. In their experiments, the lower viscosity is always on the same order as the water viscosity. A very low or high value of μ^* then implies a large $\tilde{\mu}$ and a large \tilde{Oh} . Therefore, the seemingly peculiar criterion on μ^* is actually consistent with our criterion $\tilde{Oh} < \tilde{Oh}_c$. Specifically, the upper bound $\mu^* = 10$, at which partial coalescence is arrested for drops of 50% glycerol/50% water in benzene, corresponds to $\tilde{Oh} = 2.30 \times 10^{-2}$, which is very close to our $\tilde{Oh}_c = 2.45 \times 10^{-2}$ for $\mu^* = 10$ and $\rho^* \approx 1$. The lower bound $\mu^* = 0.02$, for water drops in cyclohexanol with complete coalescence, gives $\tilde{Oh} = 0.14$, which is higher than the predicted \tilde{Oh}_c and therefore consistent with our criterion.

C. Viscoelastic fluids

In a recent experimental study, Chen *et al.*³ found that viscoelasticity in either the drop or the matrix phase tends to prolong the coalescence time, reduce the drop size ratio, and increase the minimum drop size for partial coalescence. The effect seems to be stronger if the viscoelasticity occurs in the drop than the matrix. They further proposed that the mechanism for the effect lies in the suppression of capillary instability on liquid filaments. In the present study, we have simulated the partial coalescence process when either the drop or the matrix is a polymer solution modeled as a Giesekus or Oldroyd-B fluid. For simplicity, we fix the viscosity ratio

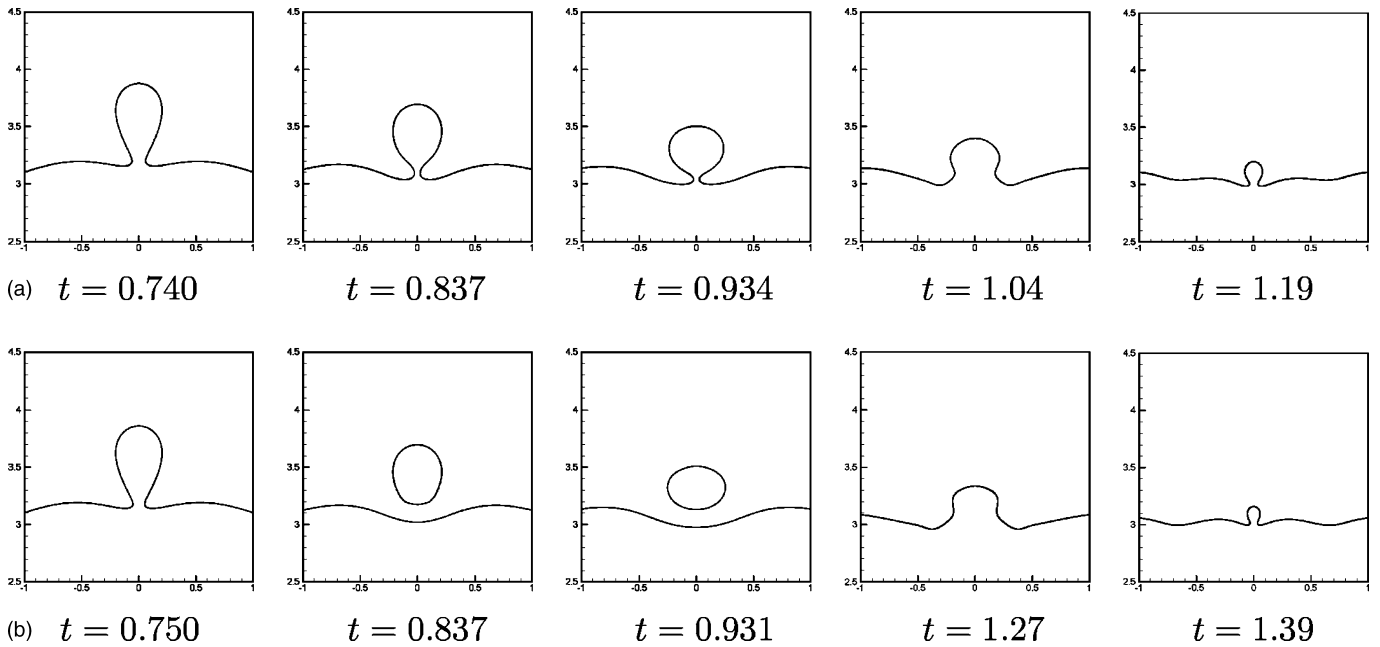


FIG. 14. Interfacial evolution for a drop coalescing with an interface. $\text{Oh}=2.0 \times 10^{-2}$, $\text{Bo}=10^{-3}$, $\rho^*=1.33$, and $\mu^*=1$. (a) An Oldroyd-B drop in a Newtonian matrix, with $\text{De}=0.1$ and the ratio between retardation time and relaxation time $\lambda_2=\mu_s/(\mu_s+\mu_p)=0.9$. (b) Both fluids are Newtonian. Time is made dimensionless by t_{ic} (enhanced online).

$\mu^*=1$ and the density ratio $\rho^*=1.33$. For viscoelastic fluids, μ^* is defined using the total (polymer plus solvent) zero-shear-rate viscosity. A small Bond number $\text{Bo}=10^{-3}$ is used as before. The Deborah number is defined as

$$\text{De} = \frac{\lambda_H}{t_{ic}} = \lambda_H \sqrt{\frac{\sigma}{\rho_1 D^3}}, \quad (12)$$

where λ_H is the polymer relaxation time.

Figure 14 compares two drop-interface coalescence sequences: in (a) the drop and lower bulk is an Oldroyd-B fluid while in (b) both fluids are Newtonian. All other conditions are the same. Partial coalescence occurs in (b) because $\tilde{\text{Oh}}=1.85 \times 10^{-2}$ is below the critical value $\tilde{\text{Oh}}_c=2.45 \times 10^{-2}$ [cf. Eq. (11) and Fig. 11]. The fluid column necks, pinches off, and forms a secondary drop. The secondary drop itself then coalesces with the interface, and this coalescence is complete in one shot because $\tilde{\text{Oh}}$ is now higher than $\tilde{\text{Oh}}_c$. The viscoelastic drop in (a) exhibits a different behavior: partial coalescence is arrested and no secondary drop is produced. Before $t=0.74$, the interface evolves in almost exactly the same way as that of the Newtonian system. But during the necking process, especially its later stage, viscoelasticity begins to play an important role. The neck gets very thin ($t=0.837-0.934$) but never pinches off. The bulb on top of the thin neck behaves as a drop; it falls under gravity onto the interface and generates a new ring of capillary wave that propagates upward along the drop surface ($t=1.04$). There is even a new episode of necking ($t=1.19$) before complete coalescence. The suppression of partial coalescence and the “secondary coalescence” of the attached bulb have been experimentally observed for drops of dilute polymer solutions.³

Figure 15 shows two snapshots of the flow and stress fields at the neck. At the earlier time ($t=0.74$), the draining

flow is appreciable while the polymer stress has not had time to develop. Because of the energy barrier discussed earlier, capillarity opposes further necking. But the flow is dominated by inertia, and the Bernoulli effect produces a low pressure inside the neck where the flow speed is high [Fig. 15(a)]. The low pressure overcomes the capillary resistance and causes the neck to pinch in further. This creates an elongational flow in the neck. By $t=0.837$, therefore, the polymer stress τ_{yyy} has grown to very high levels, with a maximum around 50 at the thinnest part of the neck. In comparison, the viscous stress has a local maximum of roughly 1. The direct consequence of this high tensile stress (or elongational viscosity) is the suppression of further stretching and thinning of the neck. Note that the downward flow in the neck is much reduced in Fig. 15(b) as compared with Fig. 15(a). Thus, viscoelasticity in the drop phase has arrested partial coalescence. The polymer tensile stress in Fig. 15(b) is reminiscent of the high viscoelastic stress that develops in polymer threads undergoing capillary breakup.³⁰ But we do not produce the “beads-on-a-string” morphology for the parameters used in this simulation. Experimentally, Chen *et al.*³ did observe beads developing on the neck that connects the drop to the lower bulk.

To quantify the viscoelastic effect, we have conducted a modest parametric study using the Giesekus model. For the Oldroyd-B model, the viscoelastic stress tends to grow to such levels as to cause numerical divergence. The Giesekus mobility parameter α moderates the elongational stress.²³ Our results show that even a small α is sufficient to restore partial coalescence. We have tested $\alpha=0.01$ and 0.1 at $\text{De}=0.1$ and 1 , $\text{Oh}=0.01$ and 0.02 , and $\lambda_2=0.8$, all of which result in partial coalescence. The sensitivity of partial coalescence to α is analogous to the capillary breakup of viscoelas-

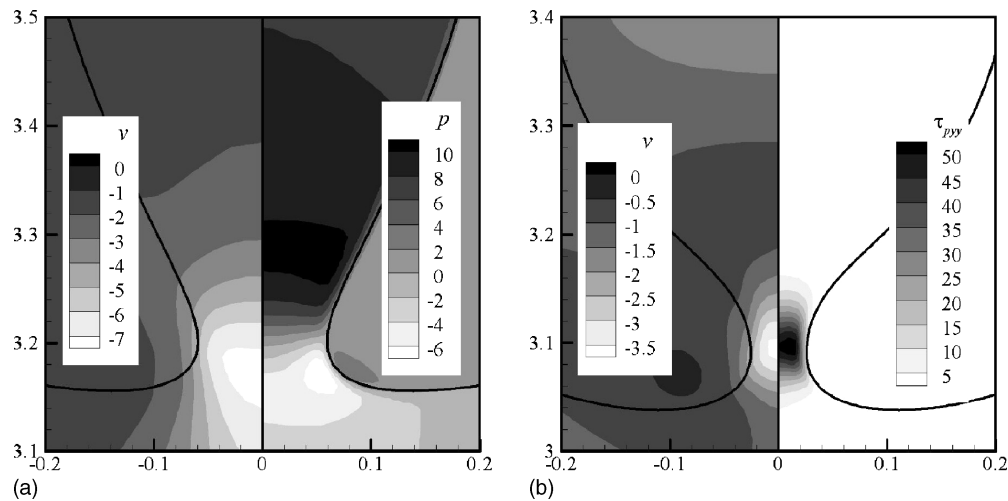


FIG. 15. Flow and stress fields around the neck of the fluid column for the simulation in Fig. 14(a). (a) Vertical velocity v_y and pressure p contours at $t=0.740$. The polymer stress is small at this stage, with a maximum of $\tau_{pyy}=4.98$. (b) Vertical velocity v_y and polymer stress τ_{pyy} contours at $t=0.837$. Velocity is scaled by D/t_{ic} and stresses by σ/D .

tic jets, where an Oldroyd-B jet does not break up while a comparable Giesekus jet does.³¹ When a viscoelastic drop does undergo partial coalescence, the tensile stress depicted in Fig. 15(b) delays the pinch-off. Thus, the coalescence time τ_c is longer than its Newtonian counterpart, and increases with decreasing α in Table I. This is in agreement with experiments.³ The drop size ratio ζ , on the other hand, essentially remains unchanged with the rheology (last column of Table I). This is because the polymer stress in the neck not only delays pinch-off, but also suppresses the draining of the drop fluid into the bulk [see Fig. 15(b)]. Thus, the Giesekus drop loses little more fluid in the final stage of pinch-off even though the process lasts longer. This appears to be at odds with the experimental finding that polymer drops tend to have somewhat lower ζ .³

If the viscoelasticity occurs in the matrix fluid rather than the drop, our simulations show that its effect is qualitatively the same. Some results are tabulated in Table I for a Newtonian drop coalescing with a Giesekus-Newtonian fluid interface. The coalescence time τ_c is longer than the Newtonian value as pinch-off is delayed, but ζ changes little. Figure 16 shows the polymer stress field around the neck before pinch-off. First, the polymer stress in the ambient fluid is restricted to a narrow region next to the interface, which, considering the axisymmetry of the geometry, constitutes a thin-walled tube that wraps around the neck of the

Newtonian fluid column. Second, at the interface the principal direction of the stress tensor is tangential, and the principal tensile stress attains its maximum at the thinnest point of the neck. Since the fluid inside the neck undergoes strong stretching, the Giesekus fluid experiences a similar deformation by way of the no-slip condition on the interface. Hence the high tensile polymer stress surrounding the interface. By the same token, this tensile stress along the interface tends to inhibit the stretching of the interface because that entails stretching of the surrounding fluid as well against the polymer stress. Thus, necking is hampered and pinch-off is delayed. This prediction is consistent with the experimental observation that adding polymer to the matrix phase delays the pinch-off of the secondary drop and even inhibits partial coalescence.³

Chen *et al.*³ observed that the viscoelasticity impacts partial coalescence more when it is in the drop than the am-

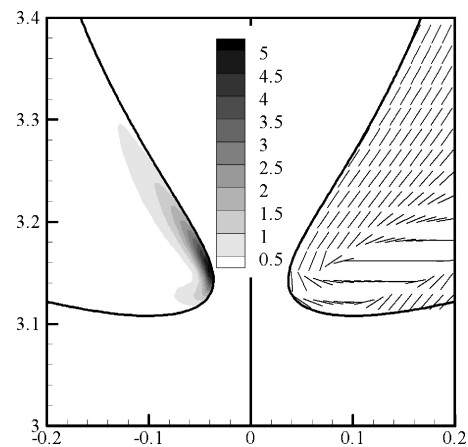


FIG. 16. Polymer stress distribution near the interface for a Newtonian drop coalescing with a Giesekus-Newtonian interface. The parameters are $Oh=2.0 \times 10^{-2}$, $Bo=10^{-3}$, $\rho^*=1.33$, $\mu^*=1$, $\alpha=0.01$, $\lambda_2=0.8$, $De=0.1$, and the dimensionless time is $t=0.776$. The right half of the plot shows the principal direction of the polymer stress while the left half shows the magnitude of the tensile stress along the principal direction.

TABLE I. Coalescence time τ_c and drop size ratio ζ for partial coalescence in Newtonian/Giesekus systems at $Oh=0.02$, $\mu^*=1$, $\rho^*=1.33$, and $Bo=10^{-3}$. $De=0.1$ and $\lambda_2=0.8$ for Giesekus fluids.

Fluid components		τ_c	ζ
Newtonian drop in Newtonian matrix		0.752	0.460
Giesekus drop in Newtonian matrix	$\alpha=0.1$	0.785	0.463
	$\alpha=0.01$	0.818	0.459
Newtonian drop in Giesekus matrix	$\alpha=0.1$	0.796	0.459
	$\alpha=0.01$	0.811	0.457

bient fluid. This is reasonable considering that in the latter case, the polymer stress influences the thinning and pinch-off of the neck *indirectly* via the interface. For reasons that are unclear at present, the data in Table I do not show a clear trend for the Giesekus drop vis-à-vis the Giesekus matrix. One indication apparently consistent with the experiment is that while partial coalescence can be completely suppressed for the Oldroyd-B drop in Fig. 14, we are unable to suppress partial coalescence with a Giesekus or Oldroyd-B matrix for a range of parameters tested.

IV. CONCLUSION

The numerical simulations are motivated by recent experiments on the coalescence between a drop and a fluid interface, and have reproduced important aspects of the experimental observations. Within the parameter ranges examined, we may summarize the numerical results as follows.

- (1) For a Newtonian drop in a Newtonian ambient fluid, our numerical package AMPHI simulates the partial coalescence process nearly to quantitative accuracy. The pinch-off of the secondary drop requires the kinetic energy of the fluids to overcome an energy barrier due to an initial increase in the interfacial area.
- (2) Partial coalescence occurs within an intermediate drop size. For Newtonian systems with small gravity effects, a “universal criterion” has been proposed in terms of the density ratio and a composite Ohnesorge number: partial coalescence occurs only if $\tilde{Oh} < \tilde{Oh}_c(\mu^*, \rho^*)$ and $\rho^* > \rho_c^*$.
- (3) Viscoelasticity in either component hinders the stretching of the neck and delays the pinch-off. Partial coalescence may be completely eliminated when the drop fluid is viscoelastic. The drop size ratio varies little with the rheological parameters.

We have to emphasize the numerical challenge in resolving interfacial phenomena that occur on a length scale comparable to the interfacial thickness. The diffuse-interface model employed here has the advantage of simulating interfacial rupture and coalescence naturally. But a downside is the loss of accuracy due to numerical diffusion when the length scale approaches that of the interfacial thickness. With adaptive meshing, the minimum length scale that AMPHI can resolve is on the order of 10^{-3} of the macroscopic length (e.g., drop diameter D). This has limited our simulations to low Bo values, and small-scale events such as pinch-off tend to take place more rapidly than in reality owing to numerical diffusion. With this caveat, we conclude that the simulations agree well with experimental observations, and provide new insights into the physics governing partial coalescence, especially the role of viscoelastic stresses.

ACKNOWLEDGMENTS

Acknowledgment is made to the Donors of The Petroleum Research Fund, administered by the American Chemical Society, for partial support of this research. J.J.F. was also

supported by the NSERC, the Canada Research Chair program, the Canada Foundation for Innovation, and the NSFC (No. 20490220). C.Z. acknowledges partial support by a University Graduate Fellowship from UBC.

- ¹G. E. Charles and S. G. Mason, “The mechanism of partial coalescence of liquid drops at liquid/liquid interfaces,” *J. Colloid Sci.* **15**, 105 (1960).
- ²X. Chen, S. Mandre, and J. J. Feng, “Partial coalescence between a drop and a liquid-liquid interface,” *Phys. Fluids* **18**, 051705 (2006).
- ³X. Chen, S. Mandre, and J. J. Feng, “An experimental study of the coalescence between a drop and an interface in Newtonian and polymeric liquids,” *Phys. Fluids* **18**, 092103 (2006).
- ⁴S. T. Thoroddsen and K. Takehara, “The coalescence cascade of a drop,” *Phys. Fluids* **12**, 1265 (2000).
- ⁵S. Tomotika, “On the instability of a cylindrical thread of a viscous liquid surrounded by another viscous liquid,” *Proc. R. Soc. London, Ser. A* **150**, 322 (1935).
- ⁶A. D. Nikolov and D. T. Wasan, “Effects of surfactant on multiple stepwise coalescence of single drops at liquid-liquid interfaces,” *Ind. Eng. Chem. Res.* **34**, 3653 (1995).
- ⁷Z. Mohamed-Kassim and E. K. Longmire, “Drop coalescence through a liquid/liquid interface,” *Phys. Fluids* **16**, 2170 (2004).
- ⁸E. M. Honey and H. P. Kavehpour, “Astonishing life of a coalescing drop on a free surface,” *Phys. Rev. E* **73**, 027301 (2006).
- ⁹P. Yue, J. J. Feng, C. Liu, and J. Shen, “A diffuse-interface method for simulating two-phase flows of complex fluids,” *J. Fluid Mech.* **515**, 293 (2004).
- ¹⁰R. Chella and J. Viñals, “Mixing of a two-phase fluid by cavity flow,” *Phys. Rev. E* **53**, 3832 (1996).
- ¹¹D. M. Anderson, G. B. McFadden, and A. A. Wheeler, “Diffuse-interface methods in fluid mechanics,” *Annu. Rev. Fluid Mech.* **30**, 139 (1998).
- ¹²J. Lowengrub and L. Truskinovsky, “Quasi-incompressible Cahn-Hilliard fluids and topological transitions,” *Proc. R. Soc. London, Ser. A* **454**, 2617 (1998).
- ¹³D. Jacqmin, “Calculation of two-phase Navier-Stokes flows using phase-field modelling,” *J. Comput. Phys.* **155**, 96 (1999).
- ¹⁴B. J. Keestra, P. C. J. van Puyvelde, P. D. Anderson, and H. E. H. Meijer, “Diffuse interface modeling of the morphology and rheology of immiscible polymer blends,” *Phys. Fluids* **15**, 2567 (2003).
- ¹⁵C. Liu and J. Shen, “A phase field model for the mixture of two incompressible fluids and its approximation by a Fourier-spectral method,” *Physica D* **179**, 211 (2003).
- ¹⁶P. Yue, J. J. Feng, C. Liu, and J. Shen, “Diffuse-interface simulations of drop coalescence and retraction in viscoelastic fluids,” *J. Non-Newtonian Fluid Mech.* **129**, 163 (2005).
- ¹⁷P. Yue, J. J. Feng, C. Liu, and J. Shen, “Interfacial force and Marangoni flow on a nematic drop retracting in an isotropic fluid,” *J. Colloid Interface Sci.* **290**, 281 (2005).
- ¹⁸P. Yue, J. J. Feng, C. Liu, and J. Shen, “Viscoelastic effects on drop deformation in steady shear,” *J. Fluid Mech.* **540**, 427 (2005).
- ¹⁹P. Yue, J. J. Feng, C. Liu, and J. Shen, “Transient drop deformation upon startup of shear in viscoelastic fluids,” *Phys. Fluids* **17**, 123101 (2005).
- ²⁰P. Yue, C. Zhou, J. J. Feng, C. F. Ollivier-Gooch, and H. H. Hu, “Phase-field simulations of interfacial dynamics in viscoelastic fluids using finite elements with adaptive meshing,” *J. Comput. Phys.* (to be published).
- ²¹C. Zhou, P. Yue, and J. J. Feng, “Formation of simple and compound drops in microfluidic devices,” *Phys. Fluids* **18**, 092105 (2006).
- ²²J. J. Feng, C. Liu, J. Shen, and P. Yue, “An energetic variational formulation with phase field methods for interfacial dynamics of complex fluids: Advantages and challenges,” in *Modeling of Soft Matter*, edited by M.-C. T. Calderer and E. Terentjev (Springer, New York, 2005), pp. 1–26.
- ²³R. B. Bird, R. C. Armstrong, and O. Hassager, *Dynamics of Polymeric Liquids, Vol. 1. Fluid Mechanics* (Wiley, New York, 1987).
- ²⁴L. A. Freitag and C. F. Ollivier-Gooch, “Tetrahedral mesh improvement using swapping and smoothing,” *Int. J. Numer. Methods Eng.* **40**, 3979 (1997).
- ²⁵V. V. Khatavkar, P. D. Anderson, and H. E. H. Meijer, “On scaling of diffuse-interface models,” *Chem. Eng. Sci.* **61**, 2364 (2006).
- ²⁶J. Eggers, “Nonlinear dynamics and breakup of free-surface flows,” *Rev. Mod. Phys.* **69**, 865 (1997).

- ²⁷F. Blanchette and T. P. Bigioni, "Partial coalescence of drops at liquid interfaces," *Nat. Phys.* **2**, 254 (2006).
- ²⁸X. Zheng, J. Lowengrub, A. Anderson, and V. Cristini, "Adaptive unstructured volume remeshing—II: Application to two- and three-dimensional level-set simulations of multiphase flow," *J. Comput. Phys.* **208**, 626 (2005).
- ²⁹C. M. Kinoshita, H. Teng, and S. M. Masutani, "A study of the instability of liquid jets and comparison with Tomotika's analysis," *Int. J. Multiphase Flow* **20**, 523 (1994).
- ³⁰J. Li and M. A. Fontelos, "Drop dynamics on the beads-on-string structure for viscoelastic jets: A numerical study," *Phys. Fluids* **15**, 922 (2003).
- ³¹M. Renardy, "A numerical study of the asymptotic evolution and breakup of Newtonian and viscoelastic jets," *J. Non-Newtonian Fluid Mech.* **59**, 267 (1995).